Toward Accurate Coastal Ocean Prediction

Peter C. Chu
Naval Postgraduate School, Monterey, CA 93943, USA

November 28, 2000

1 Introduction

Several major problems, namely, uncertain surface forcing function, unknown open boundary conditions (OBC), and pressure gradient error using the σ-coordinate, affect the accuracy of coastal ocean prediction. At open lateral boundaries where the numerical grid ends, the fluid motion should be unrestricted. Ideal open boundaries are transparent to motions. The most popular and successful scheme is the adjoint method. The disadvantages that may restrict its use are ocean-model dependency and difficulty in deriving the adjoint equation when the model contains rapid (discontinuous) processes, such as change of ocean mixed layer from entrainment to shallowing regime. Development of a ocean-model independent algorithm for determining the OBC becomes urgent.

Reduction of horizontal pressure gradient error is another key issue of using σ-coordinate ocean models, especially of using coastal models. The error is caused by the splitting of the horizontal pressure gradient term into two parts and the subsequent incomplete cancellation of the truncation errors of those parts. As advances of the computer technology, use of highly accurate schemes for ocean models becomes feasible.

2 Uncertainty of Surface Forcing

To investigate the uncertainty of surface wind forcing and its effect on the coastal prediction, the Princeton Ocean Model (POM, Blumberg and Mellor, 1987) was used with 20 km horizontal resolution and 23 sigma levels conforming to a realistic bottom topography during the life time of tropical cyclone Ernie 1996 over the South China Sea (SCS). A study (Chu, et al, 1999) shows that the root-mean-square (RMS) difference of each component (zonal or latitudinal) between the two wind data (NCEP and NSCAT) over the whole SCS during November 1996 fluctuated between 2.7 m/s to 6.5 m/s. The uncertainty of the whole SCS response to the two wind data sets were 4.4 cm for surface elevation, 0.16 m/s for surface current velocity, and 0.5°C for near-surface temperature, respectively.

P.F. Hodnett (ed.),
IUTAM Symposium on Advances in Mathematical Modeling of Atmosphere and Ocean Dynamics, 131–136.

3 Jacobian Matrix Method for Determining OBCs

Improvement of coastal prediction largely depends on determination of lateral OBCs, vector, $\mathbf{B} = (b_1, b_2, ..., b_n)$. The observation forms an m-dimensional vector (observation vector) $\mathbf{O} = (O_1, O_2, ...O_m)$, located at the interior. If **B** is given, we can solve the dynamic system and obtain the solution S. At the observational points, the solutions form a solution vector $\mathbf{S} = (S_1, S_2, ...S_m)$, which depends on **B** (Fig. 1).

It is reasonable to determine **B** with the given **O** by minimize the RMS error

$$I = \sqrt{\frac{1}{m}\sum_{j=1}^{m}(S_j - O_j)^2}. \tag{1}$$

which leads to a set of n equations implicitly solvable for $b_1, b_2, ...b_n$,

$$\sum_{j=1}^{m}(S_j - O_j)R_{ij} = 0, \qquad i = 1, 2, ..., n \tag{2}$$

where

$$R_{ij} \equiv \frac{\partial S_j}{\partial b_i}, \qquad i = 1, 2, ..., n;\ j = 1, 2, ...m. \tag{3}$$

are components of a $n \times m$ Jacobian matrix $R = \{R_{ij}\}$.

From a first guess boundary vector $\mathbf{B}^*$, a solution vector $\mathbf{S}^*$ is obtained by solving the numerical ocean model. The RMS between $\mathbf{S}^*$ and **O** might not be minimal. We update the boundary parameter vector components by increments $\{\delta b_i |\ i = 1, 2, ..., n\}$, and therefore components of the solution vector become

$$S_j = S_j^* + \sum_{i=1}^{n} R_{ij}\delta b_i + \text{ high order terms} \tag{4}$$

Substituting (4) into (2) and neglecting higher order terms leads to a set of n linear algebraic equations for $\{\delta b_i\}$,

$$\sum_{l=1}^{n} P_{il}\delta b_l = d_i, \qquad i = 1, 2, ..., n \tag{5}$$

where

$$P_{il} \equiv \sum_{j=1}^{m} R_{lj}R_{ij}, \qquad d_i \equiv \sum_{j=1}^{m} R_{ij}(O_j - S_j^*); \qquad i = 1, 2, ..., n;\ l = 1, 2, ...n. \tag{6}$$

Both O_j and S_j^* are known quantities. Therefore, the linear algebraic equations (5) have definite solutions when the Jacobian matrix $\{R_{ij}\}$ is determined and

$$\det\{P_{il}\} \neq 0 \tag{7}$$

This method was verified by a flat bay centered at 35°N and bounded by three rigid boundaries (Fig. 1). This bay expands 1000 km in both the north-south and east-west directions. The northern, southern, and western boundaries are rigid, and the eastern boundary is open. Using the optimization method, the temporally varying OBC, $\mathbf{B}(t)$, is determined. After 10 day's of integration, the magnitude of relative error

$$E^{(O)} \equiv \frac{\sum |O_j - S_j|}{\sum |O_j|} \tag{8}$$

is on the order of 10^{-4}-10^{-5} (Fig. 2), which is almost in the noise level. The Jacobian matrix method performs well even when random noises are added to the 'observational' points. This indicates that we can use real-time data to invert for the unknown open boundary values.

4 High-Order Difference Schemes

4.1 A Hidden Problem

Improvement of the prediction also partially depends on the selection of the discretization schemes. Most coastal models use second-order difference schemes (such as second-order staggered C-grid scheme) to approximate first-order derivative

$$\left(\frac{\partial p}{\partial x}\right)_i \simeq \frac{p_{i+1/2} - p_{i-1/2}}{\Delta} - \frac{1}{24}\left(\frac{\partial^3 p}{\partial x^3}\right)_i \Delta^2, \tag{9}$$

where p, Δ represent pressure and grid spacing. This scheme uses the local Lagrangian Polynomials whose derivatives are discontinuous.

4.2 Combined Compact Scheme

Recently, Chu and Fan (1997, 1998, 1999, 2000) proposed a new three-point combined compact difference (CCD) scheme,

$$\left(\frac{\delta f}{\delta x}\right)_i + \alpha_1 \left(\left(\frac{\delta f}{\delta x}\right)_{i+1} + \left(\frac{\delta f}{\delta x}\right)_{i-1}\right) + \beta_1 h \left(\left(\frac{\delta^2 f}{\delta x^2}\right)_{i+1} - \left(\frac{\delta^2 f}{\delta x^2}\right)_{i-1}\right) + \ldots$$
$$= \frac{a_1}{2h}\left(f_{i+1} - f_{i-1}\right)$$

$$\left(\frac{\delta^2 f}{\delta x^2}\right)_i + \alpha_2 \left(\left(\frac{\delta^2 f}{\delta x^2}\right)_{i+1} + \left(\frac{\delta^2 f}{\delta x^2}\right)_{i-1}\right) + \beta_2 \frac{1}{2h} \left(\left(\frac{\delta f}{\delta x}\right)_{i+1} - \left(\frac{\delta f}{\delta x}\right)_{i-1}\right) + \ldots \tag{10}$$
$$= \frac{a_2}{h^2}\left(f_{i+1} - 2f_i + f_{i-1}\right)$$

to compute f_i' , $f_i'', ...f_i^{(k)}$ by means of the values and derivatives at the two neighboring points. Moving from the one boundary to the other, CCD forms a global algorithm to compute various derivatives at all grid points, and guarantees continuity of all derivatives at each grid point.

4.3 Seamount Test Case

4.3.1 Model Description

Suppose a seamount (Fig. 3) located inside a periodic f-plane ($f_0 = 10^{-4}\mathrm{s}^{-1}$) channel with two solid, free-slip boundaries along constant y. Unforced flow over seamount in the presence of resting, level isopycnals is an idea test case for the assessment of pressure gradient errors in simulating stratified flow over topography. The flow is assumed to be reentrant (periodic) in the along channel coordinate (i.e., x-axis). We use this seamount case of the Semi-spectral Primitive Equation Model (SPEM) version 3.9 (Haidvogel et al., 1991) to test the new difference scheme.

4.4 Temporal Variations of Peak Error Velocity

Owing to a very large number of calculations performed, we discuss the results exclusively in terms of the maximum absolute value the spurious velocity (called peak error velocity) generated by the pressure gradient errors. Fig. 4 shows the time evolution of the peak error velocity for the first 20 days of integration with the second-, fourth-, and sixth-order ordinary schemes. The peak error velocity fluctuates rapidly during the first few days integration. After the 5 days of integration, the peak error velocity show the decaying inertial oscillation superimposed into asymptotic values. The asymptotic value is around 0.19 cm/s for the ordinary scheme and 0.15 cm/s for the compact scheme. For the sixth order difference the asymptotic value is near 0.04 cm/s for the ordinary scheme and 0.02 cm/s for the compact scheme.

5 Conclusions

(1) The surface forcing function contains uncertainty. The difference between commonly used NSCAT and NCEP surface wind data is not negligible. The response of the South China Sea to the uncertain surface forcing is also evident. Therefore, it is quite urgent to study the model sensitivity to surface boundary conditions.

(2) The Jacobian matrix method provides a useful scheme to obtain unknown open boundary values from known interior values. The optimization method performs well even when random noises are added to the 'observational' points. This indicates that we can use real-time data to invert for the unknown open boundary values.

(3) The σ-coordinate, pressure gradient error depends on the choice of difference schemes. Fourier analysis shows that the fourth-order scheme may reduce

the truncation errors by 1-2 order of magnitude compared to the second-order scheme, and the sixth-order scheme may reduce the truncation errors further by 1-2 order of magnitude compared to the fourth-order scheme. Within the same order of the difference the combined compact scheme leads to a minimum truncation error. The compact scheme may reduce near 55% error, and the combined compact scheme may reduce near 84% error compared to ordinary sixth-order difference scheme.

6 ACKNOWLEDGMENTS

This research is sponsored by the Office of Naval Research, Naval Oceanographic Office, and Naval Postgraduate School.

References

[1] Blumberg, A.F., and Mellor, G.L. (1987) A description of a three-dimensional coastal ocean circulation model. *Three Dimensional Coastal Ocean Models,* edited by N.S. Heaper, American Geophysical Union, 1-16.

[2] Chu, P.C., and Fan, C. (1997) Sixth-order difference scheme for sigma coordinate ocean models. *Journal of Physical Oceanography*, **27**, 2064-2071.

[3] Chu, P.C., and Fan, C. (1998) A three-point combined compact difference scheme. *Journal of Computational Physics*, **140**, 1-30.

[4] Chu, P.C., and Fan, C. (1999) A non-uniform three-point combined compact difference scheme, *Journal of Computational Physics*, **148**, 663-674.

[5] Chu, P.C., and Fan, C. (2000) A staggered three-point combined compact difference scheme, *Mathematical and Computer Modeling*, **32**, 323-340.

[6] Chu, P.C., Chen, Y.C. and Lu, S.H. (1998) On Haney-type surface thermal boundary conditions for ocean circulation models. *Journal of Physical Oceanography*, **28**, 890-901.

[7] Chu, P.C., Fan, C. and Ehret, L. (1997) Determination of open boundary conditions with an optimization method. *Journal of Atmospheric and Oceanic Technology*, **14**, 723-734.

[8] Chu, P.C., Lu, S.H. and Liu, W.T. (1999) Uncertainty of the South China Sea prediction using NSCAT and NCEP winds during tropical storm Ernie 1996. *Journal of Geophysical Research,* 104, 11273-11289.

[9] Haidvogel, D.B., Wikin, J.L., and Young, R. (1991) A semi-spectral primitive equation model using vertical sigma and orthogonal curvilinear coordinates. *Journal of Computational Physics*, **94**, 151-185.

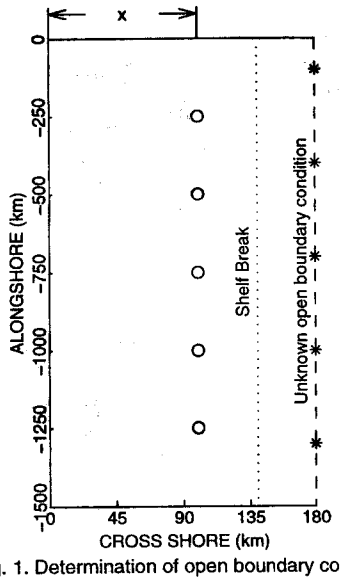

Fig. 1. Determination of open boundary condition

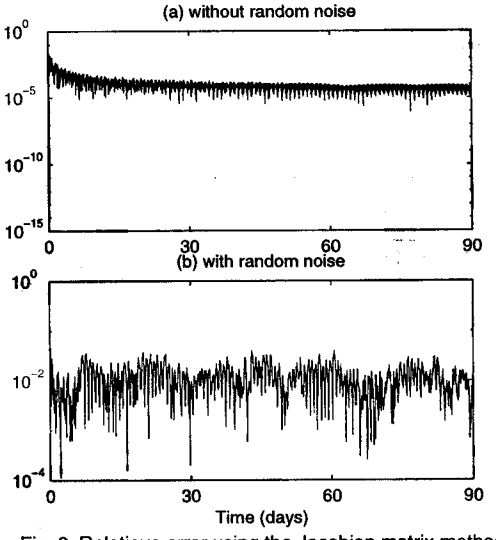

Fig. 2. Relatiove error using the Jacobian matrix method.

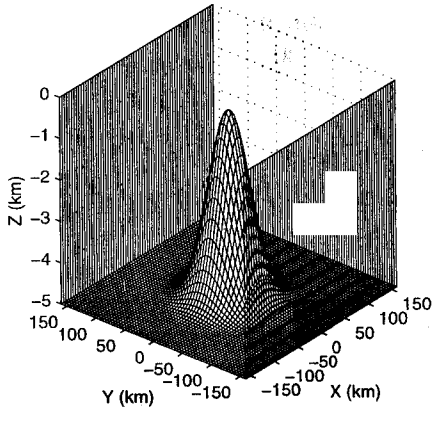

Fig. 3. Seamount geometry

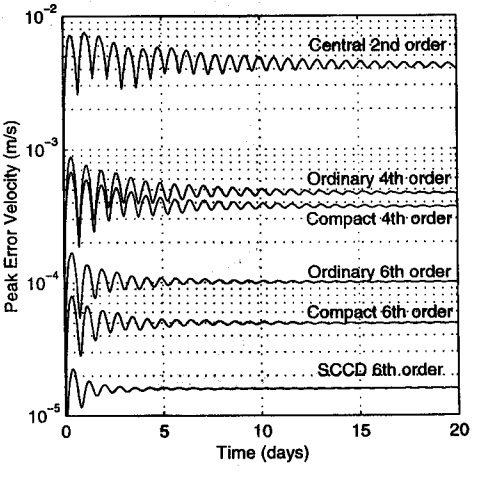

Fig. 4. Peak error velocity for different order schemes